TanDEM-X Water Indication Mask: Generation and First Evaluation Results

Anna Wendleder, Birgit Wessel, Achim Roth, Markus Breunig, Klaus Martin, and Susanne Wagenbrenner

***Abstract*—The German SAR interferometry mission TanDEM-X performed on two TerraSAR-X satellites flying in close formation will provide a global Digital Elevation Model (DEM). A by-product is so-called the Water Indication Mask (WAM). The purpose of this supplementary information layer is to support the DEM editing process. Water surfaces usually show lower coherence in an interferometric data set due to temporal de-correlation and low backscattering. Consequently the corresponding elevation values derived from the interferogram are random and produce a virtual relief. This paper introduces the operational water body detection workflow that synergistically evaluates amplitude and coherence information. The presented results of two test sites reveal that the methodology is globally applicable, classifications are highly accurate and the algorithm is appropriate for operational image processing. The water body detection consists of two steps: the Water Body Detection (WBD) derived of one single DEM scene and the mosaicking of multiple WBD to a single Water Indication Mask (WAM). The fusion strategy for the final TanDEM-X WAM considers all WBD acquired at different times in two global coverages and bases on a fusion by union containing the results of the amplitude and the coherence.**

***Index Terms*—Amplitude, coherence, DEM editing, TanDEM-X, water body detection.**

I. Introduction

THE TanDEM-X satellite was launched on June 15th 2010 and is now flying in a close formation with its twin satellite TerraSAR-X that is in space since June 21st 2007. Both satellites are part of the TanDEM-X mission and acquire operational high resolution single-pass across-track SAR interferometry DEMs over the whole of Earth's land surface. The major goal is the generation of a seamless, accurate and high resolution global Digital Elevation Model (DEM) with an unprecedented combination of coverage and height accuracy [1]. The absolute horizontal and vertical accuracy will be 10 m with a 12 m posting. In 2011, within one year, a first global coverage was acquired. The acquisition of a second global coverage started in April 2012 and will be completed by the begin of 2013. Both coverages plus additional data takes of difficult terrain will be processed to the final TanDEM-X DEM product which shall be made available in 2014. Due to the worldwide coverage and the high resolution of TanDEM-X, 600 scenes per day must be processed. This large volume of data can only be handled with a fully automated process, but with losses of the final product's quality.

This paper addresses the TanDEM-X Water Indication Mask (WAM) which is a part of the final TanDEM-X DEM product. The purpose of the WAM is to detect the disturbed surface of water bodies that will remain in the final DEM layer and hence to support a subsequent DEM editing like flattening of rough water bodies. Most applications like ortho-rectification of remote sensing data [2], [3] or any geo-application like hydrological modelling [4], [5] require flat and smooth water areas. The data set will not provide a global and complete water mask. But with a resolution of 12 m the WAM will offer an outstanding, precise and up-to-date information layer for many geo-scientific applications.

The involved system within the DEM production chain is the 'DEM Mosaicking and Calibration Processor' (MCP). The MCP is responsible for providing a consistent global DEM product [6] and is the subsequent processor to the 'Integrated TanDEM-X Processor' (ITP) [7] which performs the interferometric processing. The *water body detection* [8] is part of the DEM preparation process that provides important parameters, statistics and quality indicators like *control and tie-point extraction* [9] and *height discrepancy detection* due to phase unwrapping errors. The DEM preparation process analyses every single DEM scene individually. The purpose of this process is to deliver the complete input for the later on DEM calibration and mosaicking up to the resulting final DEM product [9], [10]. In the mosaicking step all Water Body Detection masks (WBD) of the first and the second global coverage derived in the DEM preparation process are fused to one final WAM.

The following sections are organized as follows. Section II explains the TanDEM-X specific constraints for deriving water bodies. A brief overview of current approaches of water body detection from SAR data is given in Section III. The methodology for water body detection and the water body mosaicking is presented in Section IV. In Section V, the used data set and study area are explained and the results of the Water Body Detection mask on two different test sites and equally the result of a mosaicked Water Indication Mask of one test site is evaluated. A conclusion is given in Section VI.

Manuscript received October 07, 2011; revised January 17, 2012 and April 11, 2012; accepted July 17, 2012. Date of publication September 14, 2012; date of current version March 11, 2013. This work was supported in part by the German Federal Ministry for Economics and Technology (Förderkennzeichen 50 EE 1035). The TanDEM-X project is partly funded by the German Federal Ministry for Economics and Technology (Support code 50 EE 1035).

A. Wendleder, B. Wessel, A. Roth, M. Breunig, and S. Wagenbrenner are with the German Remote Sensing Data Center, German Aerospace Center (DLR), 82234 Wessling, Germany (e-mail: anna.wendleder@dlr.de; birgit.wessel@dlr.de; achim.roth@dlr.de; markus.breunig@dlr.de; susanne.wagenbrenner@dlr.de).

K. Martin is with the Company of Remote Sensing and Environmental Research (SLU), 81243 München, Germany (e-mail: klaus.martin.slu@t-online.de).

Color versions of one or more of the figures in this paper are available online at http://ieeexplore.ieee.org.

Digital Object Identifier 10.1109/JSTARS.2012.2210999

II. Constraints of the Water Body Detection From TanDEM-X Data

At the beginning of the TanDEM-X mission the size of water bodies and island presented in the DEM were specified. The minimum mapping unit in the TanDEM-X water indication mask for lakes and rivers are two hectares which corresponds to 20,000 m^2. Though, the minimum mapping unit for islands is one hectare [11]. This corresponds to an area of 100 m $\times$ 100 m, resp. 1,000 m $\times$ 10 m. The former linear definitions, e.g. for water bodies a minimum of 300 m and for islands a minimum of 150 m major axis, was exchanged by this area measure due to different geometrical forms of water bodies. Water bodies and lake heights are not flattened in the final TanDEM-X DEM.

A. Water Appearance in Coherence and Amplitude Data

The very noisy appearance of water bodies in the DEM is caused on one hand by the low backscatter of ideally smooth water surfaces for the X-band. On the other hand, due to the small but noticeable along-track baseline structural changes of the water surface within this small time span causes the backscattered signals to de-correlate. Low coherence can be caused by the SAR imaging geometry and volume scattering, too [12]. Due to the two satellites formation TanDEM-X is a single-pass like mission but with a time lag varying between 0 and 50 milliseconds in along-track. At the equator, the along-track baseline has its maximum and decreases towards the pole. Bamler *et al.* confirms that water surfaces decorrelate within tens of milliseconds [13]. Thus, an analysis was made when open water begins to decorrelate to use this information for the water body detection. But it turned out that all along-track baselines below 10 ms were acquired at the poles in winter and the water was frozen. Above 10 ms the water already clearly decorrelates. Already some SRTM data with an effective time lag of about 0.5 ms begin to show decorrelations over the open sea. So, it is assumed that the time lag for water decorrelation is far below 10 ms along-track baseline and could not further be specified by the standard TanDEM-X DEM acquisitions. Conversely, the coherence image can be used for TanDEM-X as an information layer to achieve reliable results for serious detection of open water bodies. In winter season however coherence is preserved when rivers and lakes are frozen. 87% of the TanDEM-X acquisitions in the northern hemisphere above 60° latitude are acquired during winter season. In such cases the water body detection *using the coherence information* does not represent the water bodies correctly, but in view of the DEM quality, the measured heights provide reasonable elevation values. As the second acquisition has started in April 2012, more open water is expected to be detected in the second coverage. The WAM will contain the water detection mask of the first and the second global coverage.

In SAR amplitude data water bodies often appear dark and homogeneous due to specular reflectance. In this case, the water bodies can easily be detected with a threshold method applied on the amplitude image. But also the SAR amplitude has its limitations. Surfaces of similar roughness for the X-band like streets, runways or dry sand can be misclassified. On the other side, water can also appear brighter and with texture or pattern. Wind and waves produce a rougher surface which causes a higher backscattering to the sensor. Large water areas in coastal regions are more susceptible to the wind than small lakes in the inland [14]. Hence, this paper presents the combination of the amplitude and the coherence threshold method applied for the whole land surface for the first time.

B. Consideration of Temporal Variations Between Adjacent Acquisitions

The TanDEM-X acquisition planning optimizes the geometric constellation of the two satellites. Furthermore, several limited resources like on-board storage capacity, instrument operating time and data downlink are further acquisition constraints with respect to the achievement of a global coverage within one year. As a consequence, the time span between the acquisitions of neighbouring TanDEM-X data takes can vary between days, weeks and even months. In between, however, water bodies are affected by effects like tides, flooding, seasonally changing water levels, rain fall or aridity, snow and ice coverage and even phenological effects. In addition, at least two DEM coverages are planned that are acquired with a time-span of approximately one year. All these changes will affect the water body detection and consequently, the final WAM has to compile more heterogeneous information than e.g. the 11 days lasting SRTM (Shuttle Radar Topography Mission) in 2000 [15].

III. A Review of Methodology for Water Body Detection in SAR Data

A. SAR Backscatter

Mapping smooth water bodies is a relatively straightforward task using an amplitude threshold method. This pixel-based method is computationally relatively inexpensive and hence suitable for rapid mapping purpose. The approaches shown in [16] and [17] are mainly concentrating on backscattering analysis using amplitude imagery and different threshold techniques. The active contour models improve the delineation of rough water [18]–[20]. Hahmann confronts the parametric active contours and the geometric contours [19]. The advantage of the parametric active contours is a good performance for smooth as well as for rough water bodies. Unfortunately, the algorithm is limited because of focusing on individual small scale areas of interest. The geometric active contour delineates water surfaces roughened by wind and waves only incomplete and unsatisfactory. Both methods are implemented mostly semi-automatically and an interaction for the selection of training samples to distinguish land and water is indispensable. Due to the large computing time and the manual interaction this method is not near-real-time capable.

B. SAR Coherence

Very little literature can be found using coherence threshold method for improving water body delineation [21], [22]. This technique is only applicable with multi-pass interferometry, i.e. with tandem data acquired in a short time lag. Nico and Pappalepore used the coherence thresholding with auxiliary information of the amplitude thresholding [21]. Onana exploits am-

plitude and coherence data of ERS-1/ERS-2 jointly using two-class fuzzy classification on the filtered coherence image and extracting linear features on the amplitude image [23]. The final step is the merging of both information layers. A hybrid approach is used to exploit the coherence image for an approximate detection and improving the result with the amplitude image. This method obtains good results particularly in a rain forest context. Results using only the amplitude image showed that thin linear features are hardly detected and the lack of the spatial coherence information leads to an inefficient classification result.

SRTM was the first space borne mission to generate a seamless and a high-precision topographic map of the Earth's land surface. But due to the short along-track baseline of 7 m of two InSAR (Interferometric Synthetic Aperture Radar) images the water was coherent [24].

IV. Methodology

Taking into account the constraints for water body detection from TanDEM-X described in Section II a robust, transferable and high-efficient approach was implemented [9]. This fully automated process enables to handle the large volume of data. In the following, two terms are used and described: 'water body detection mask' (WBD) for the water mask derived from one single DEM scene (Section IV-A) and 'water indication mask' (WAM) for the final mosaicked water mask (Section IV-B).

A. Water Body Detection Using SAR Amplitude and Coherence Information

The method is divided into the water body detection itself and a pre selection step for excluding non-water zones. Fig. 1 shows the workflow of the processing chain. At first, a median filter is applied to the amplitude and the coherence images in order to reduce speckle noise and minimize classification errors. A filter size of 5 pixels $\times$ 5 pixels, which corresponds to 25 m $\times$ 25 m, provided the best result in the shortest calculation time. Then, a threshold method is applied on the amplitude and the coherence image. Kittler and Illingworth recommend employing the unique internal minimum value between two peaks in a case of histogram bimodality because it corresponds to the optimum threshold value for the segmentation of connected objects [25]. For TanDEM-X amplitude data, however, the internal minimum value for the separation of water and land is mostly absent due to rough water surface. An individual interactive adjustment of the threshold value for every amplitude image is not applicable because of the huge amount of data to be processed. Alternatively, two fix threshold values are used to account for different conditions and features of landscape. The first one refers to low SAR backscattering which ideally corresponds to smooth, black water surfaces and therefore is more reliable. Whereas the second one takes effect when water bodies show a rougher and therewith brighter surface at the time of acquisition and is hence a weaker threshold value. These two threshold values were determined empirically analyzing 1,700 randomly globally distributed amplitude images. The two threshold values $\sim$40 and $\sim$60 in digital numbers have been chosen for the segmentation. Both values can be converted

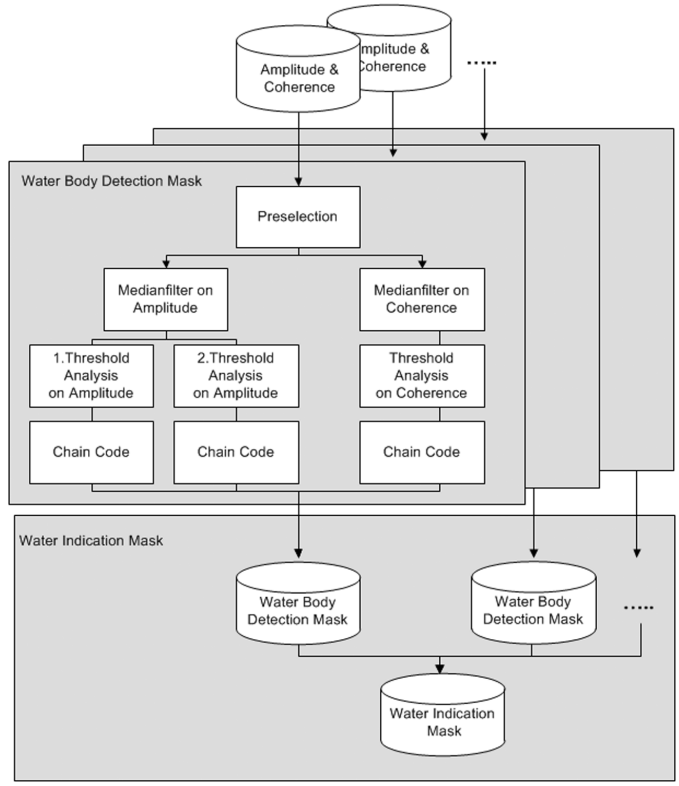

Fig. 1. Workflow of the Water Body Detection mask and of the resulting final Water Indication Mask.

to -18 dB and -15 dB in radar brightness with following formula of reference [26]

$$\beta_0 = calibrationFactor \cdot DN^2 \tag{1}$$

The first inspection of TanDEM-X data showed that in arid areas water areas are mostly lighter than in mid-latitudes, i.e. the weak threshold finds more water than the reliable one. In mid-latitudes and mountainous areas the water bodies found with the weak threshold are often misclassifications due to radar shadow. Nevertheless, the consideration of two thresholds is valuable and provides beneficial information for post-processing.

The coherence images of the previously mentioned 1,700 data sets were additionally analyzed in order to identify the most suited coherence threshold, too. The SRTM Water Body Data (SWBD) [27] served as reference for the separation of water and land pixels. The advantage of SWBD is its global coverage below 60° latitude, the consistent and homogenous water editing [28] and the similar imaging radar of both missions (SAR and InSAR). For every coherence image, the mean value of all water pixels classified in SWBD is calculated and plotted in a histogram (Fig. 2). Obviously, the corresponding coherence values do not follow the Gaussian distribution. Therefore, established criteria for thresholding like 3σ are not applicable. 3σ would mean a threshold of 0.68 which would lead to significant misclassifications particularly in forested areas. Since the histogram in Fig. 2 shows clearly a decrease of coherence value for water pixels in the range from 0.23 to 0.3, a set of analyses investigated to determine the coherence threshold empirically. Visual inspection showed that in arid

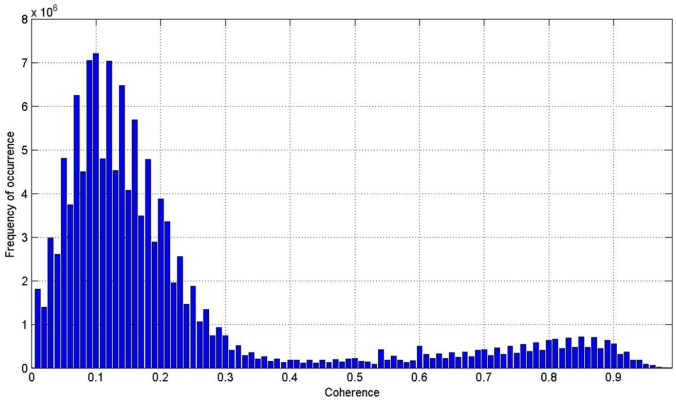

Fig. 2. Histogram of coherence for SRTM water pixels. For this statistic, 1700 globally random distributed TanDEM-X scenes are used. The coherence values between 0 and 0.3 represent water, the coherence values between 0.6 and 1 represent land and hence misclassifications due to SWBD.

areas and savannahs the coherence behaves mainly binary and the resulting water masks did not differ significantly. In mid-latitudes with varying land cover the higher threshold values like 0.3 showed much more misclassifications. In particular the coherence of forested areas can fall below 0.3. As a compromise the threshold value 0.23 was selected.

After the thresholding, a so-called chain code [29] is applied to eliminate small water bodies due to remaining speckle noise and to ensure the minimum mapping unit requirement of one respectively two hectare [11]. The chain code bases on the connected component and treats every patch separately. In contrast to the connected component, the chain code bases not on the relation of the neighbouring pixels but it circulates the boundary of every patch. As soon as the chain code is once again at the starting point area and perimeter of every patch are known. Water bodies or islands that are smaller than the minimum mapping unit are excluded from the WBD.

Finally, all three threshold results are stored in the single scene based WBD in a way that the result for each threshold is preserved. The detection results of the proposed amplitude and coherence threshold method and also the combined results are discussed with the help of two study areas in Section V.

In order to minimize computing time as well as misclassifications two additional information layers are employed to exclude non-water zones. The first set of information layers is SWBD and MODIS (Moderate-resolution Imaging Spectrometer)/Terra Land Cover Types to identify permanently frozen and desert areas. MODIS consists of the two classes '*Snow and Icy Area*" and '*Unvegetated/Barren or Sparsely Vegetated Area*' and presents the minimum spatial extent form the years 2001–2004 [14]. Frozen areas induce a high coherence, i.e. the DEM is already flat and needs no editing afterwards. Desert areas often have a low backscatter and coherence due to the absorption of the signal. Both lead to misclassifications in the amplitude as well as in the coherence image. With the help of SWBD and MODIS as reference data the correctness of the water body detection mask can be increased—with the lack of completeness. But the probability that a water body is ignored is very low in those areas. Especially, as the water body detection is performed whenever at least one pixel of the scene is lying within one of the two reference data sets as '*Water Potentially Existent*'. Beyond the coverage of SRTM this exclusion is not executed.

The second information layer is SRTM DEM to identify steep slope and hence to distinguish between radar shadows and water areas. The inclination layer is calculated in a 3×3 pixel window, which corresponds to 15 m $\times$ 15 m, using the equations of [30]. All areas with a slope higher than 20° are excluded from the water body detection. The consideration of smaller slopes like e.g. 7° would increase the risk of misclassifications caused by different water levels during the SRTM and TanDEM-X mission. The TanDEM-X DEM cannot be used as the surfaces of water areas are still rough and provide a random relief. Additionally, all areas already identified as shadow during the DEM generation within previous ITP processing are excluded for water detection.

B. Mosaicking of Water Body Detection to the Water Indication Mask of the TanDEM-X DEM Product

Finally, all Water Body Detection masks of the first and the second acquisition plus possible additional acquisitions of difficult terrain are mosaicked to the final product, the Water Indication Mask (WAM). The name already suggests that this final mask just gives an *indication* for water but no water inventory mask. The indication for water is given by the sum of the counts of the individual detections for each pixel, the more counts the more secure the detection of water is. The resulting WAM provides the counts separately for each threshold—the two amplitude and the one coherence thresholds. A maximum number of three counts are possible for each threshold as this corresponds to the maximum findings: one in each of the first and the second globally coverages and one in an additional coverage in difficult terrain or alternatively one in the 4 km overlap in range of neighbouring acquisitions. A combination in this way corresponds to a fusion by union. The advantage of this combination is the minimization of outliers. For example if one threshold analyses or one WBD does not represent the real water area due to coherent water, missing SAR backscattering or seasonality, the classification results of the other information layer or acquisitions will compensate the missing or wrong classification result. The disadvantage of this combination is that it is not easy to interpret when annotated in an 8-bit file as the information is encoded bit-wise. For example, if the input for the WAM is only one WBD of a single DEM scene, only six combinations of classification results are possible. The pixel is described by detection with the first amplitude threshold and/or the second amplitude threshold and/or coherence threshold. As soon as two or rather three acquisitions at different times are available as input, the combinations increase up to 2^6. In this case, the pixel is not only described by the three different threshold analyses, but also by the number of the classifications. Reference [11] illustrates the bit annotation of the WAM. The general idea is to keep as much extracted information as possible to allow individual post-processing for different applications. Therefore, the acquisition time of every DEM scene used in the mosaicking is annotated. This information enables the consideration of temporal and seasonal conditions.

V. Discussion of Results

A. Study Area and Data Set

In order to prove the quality and transferability of the water detection method two study areas were selected. The first one is located at the German Bight along the coastline of Northern Germany and Southern Denmark. Tidal impacts along the coastline and mudflat can be observed within the complete study area and cause high short time water level dynamics between rising and falling tide. This test site is used for the evaluation of the water mask derived of one single DEM scene and for the evaluation of the mosaicked water mask derived of 46 DEM scenes. The data of the first mentioned, the WBD, are acquired in January 2011 at low tide; the data of the latter mentioned, the WAM, are acquired between 20th October 2010 and 9th December 2011. The second study area is located in the south-west of Orlando, Florida, near Lake Apopka and the natural reserve of Lake Louisa State Park. The terrain is relatively flat and characterised by wetlands, open water, marsh and flooded vegetation. The challenge here is to detect all these different water bodies correctly. The data was acquired in February 2011.

The reference data for the study area in North Germany were provided by the Federal Agency for Cartography and Geodesy (BKG). The corresponding vector layer of the Authoritative Topographic-Cartographic Information System (ATKIS) consists of up-to-date information about spatial location, geometric type and descriptive attributes of all water bodies like river, ocean, canal, and inland lake. The data represent the maximum water level, i.e. during high tide. The information is derived from the topographical map with a scale of 1:25,000 m and has accuracy better than 3 m [31]. The National Hydrography Dataset (NHD) provided by the US Geological Survey (USGS) is the reference for the Florida study area. It considers only freshwater bodies so that ocean coastlines as well as lagoons are missing. The vector layer bases on 1:24,000 scale topographic mapping. According to USGS, for horizontal accuracy, at least 90% of random points tested are within 0.02 inch, i.e. 0.05 cm, of their true position [32]. In contrast to those high-resolution reference data global reference data sets like GSHHS (Global Self-consistent Hierarchical High-Resolution Shoreline Database) or NOAA (National Oceanic and Atmospheric Administration) are not that suited for a detailed accuracy evaluation. The problematic consists in the small scale of the reference data in contrast to the high resolution of TanDEM-X. Studies at different test sites showed that most global reference data are inaccurate (generalisation of the coastlines), horizontally shifted (geometry and tides) or show artefacts. However, the largest problem is the comparison of two data sets with different water level due to temporal changes.

B. Evaluation of Scene-Based Water Body Detection Mask

The WBD is evaluated for both study areas near Hamburg and Orlando. A quantitative accuracy assessment has been performed by determining completeness and correctness separately for the WBD derived from the amplitude and the coherence images. The completeness says how complete the extracted data are. It is defined with the percentage of the extracted data which lies within the reference data and the complete area of reference:

$$completeness = \frac{\text{area of extraction within reference}}{\text{area of reference}} \cdot 100 \quad (2)$$

The correctness says how correct the extracted data are. It represents the percentage of correctly extracted water areas lying within the reference area and the complete area of extraction:

$$correctness = \frac{\text{area of extraction within reference}}{\text{area of extraction}} \cdot 100 \quad (3)$$

Fig. 3 shows the study area around the river Elbe in the west of Hamburg, Germany, with the amplitude image (Fig. 3(a)), coherence image (Fig. 3(b)), the WBD derived from the amplitude image with the reliable threshold value, displayed in dark blue, and the weak threshold value, displayed in light blue (Fig. 3(c)) and the WBD derived from the coherence image (Fig. 3(d)). The evaluation results of this study area are given in Table I. For this evaluation the results of both amplitude thresholds are combined to one WBD that means all areas in light and dark blue would be delineating in one colour. All water bodies in the amplitude and the coherence image appear smooth and dark without any disturbances caused by wind, coherent water or

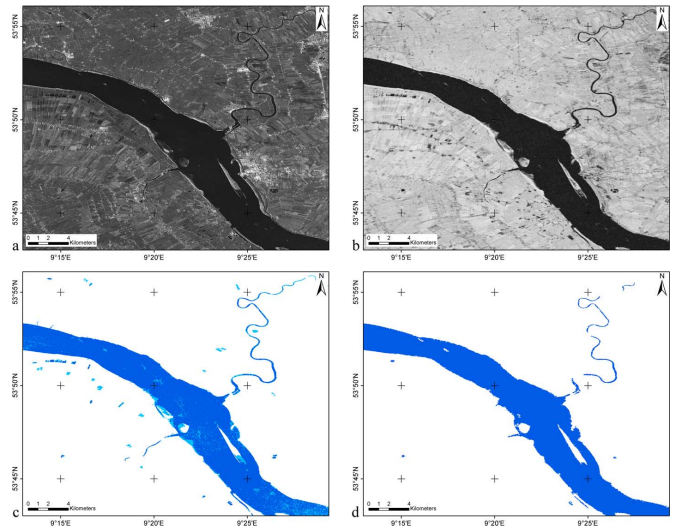

Fig. 3. (a) Amplitude image of the first study area around the river Elbe in the west of Hamburg, Germany, acquired on 27th January 2011, (b) corresponding coherence image, (c) Water body detection mask derived from the amplitude image: first amplitude threshold detections displayed in dark blue, second's in light blue, (d) Water body detection mask derived from the coherence image.

TABLE I
Evaluation Results of the Scene-Based Water Body Detection for the Two Study Areas Separated for the Water Body Detection Mask Derived of Amplitude, Coherence and the Combined Amplitude and Coherence Thresholding

		Completeness	**Correctness**
Hamburg, Germany	Amplitude	88.1 %	92.5 %
	Coherence	80.9 %	98.7 %
	Amplitude + Coherence	88.2 %	92.3%
Orlando, USA	Amplitude	70.8 %	71.1 %
	Coherence	63.8 %	93.4 %
	Amplitude + Coherence	70.8 %	71.1 %

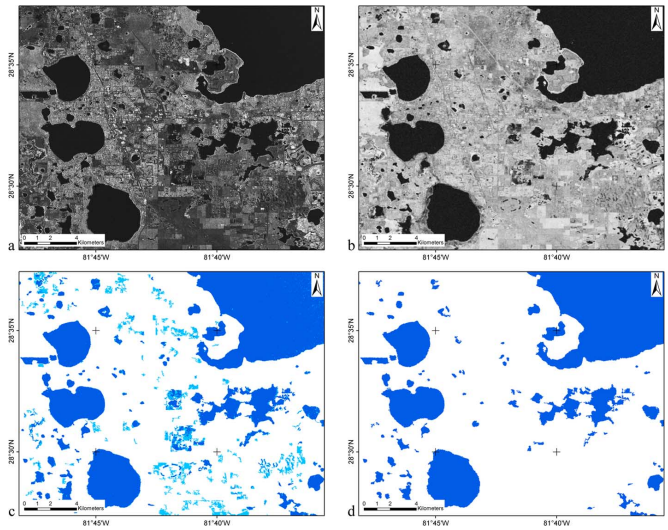

Fig. 4. (a) Amplitude image of the second study area around Lake Apopka in the west of Orlando, USA, acquired on 12th February 2011, (b) corresponding coherence image, (c) Water body detection mask derived from the amplitude image: first amplitude threshold detections displayed in dark blue, second's in light blue, (d) Water body detection mask derived from the coherence image.

other effects. The visual comparisons of Fig. 3(c) and 3(d) show that the river Elbe is classified with both amplitude thresholds as good as with the coherence threshold. One of the differences consists in the small river in the upper right of both images which is only continuously classified as water in the amplitude derived water mask. Hence the completeness of the amplitude derived water mask is greater. Another difference lies in the agricultural areas (light blue) in the left part which are misclassified as water with the weak amplitude threshold but not with the coherence threshold. The agricultural areas are not delineated in the reference data. Therefor the correctness of the coherence derived water mask with 98.7% is greater than the one of the amplitude derived water mask with 92.5%. The third row of Table I shows the overall accuracy of the combined WBD of the amplitude and the coherence thresholding by union. As the amplitude derived water mask has the maximal extent and implies the coherence derived water mask the completeness is mainly influenced by the amplitude.

This comparison is executed with water bodies with a size greater than 2 hectares according to the minimum mapping unit. As the ATKIS reference data delineates all water bodies, even the ones smaller than two hectares, small water bodies were eliminated from the reference. Furthermore, the reference data represents the water level of high tide; the TanDEM-X data is acquired during the low tide. This difference cannot be eliminated and must be considered.

Fig. 4 shows the study area near Lake Apopka in the west of Orlando, USA. The evaluation results are displayed in Table I. As well as in the test area near Hamburg, the water bodies appear dark and the result of the amplitude and the coherence derived water mask show a similar result. Equally in this study area the agricultural areas are classified as water with the weak threshold value. The low completeness of 70.8% of the amplitude derived water mask and 63.8% of the coherence derived water mask is caused by seasonal differences between the acquisitions of TanDEM-X and the reference data. According to the annotation of the reference data they were acquired during summer season while TanDEM-X observed the area in winter. The rainy season in Florida is the summer while winter is dryer. Due to the misclassified water bodies of the weak amplitude threshold (displayed in light blue in Fig. 4(c)), the correctness of the coherence derived water mask is with 93.4% greater than the amplitude derived water mask with a value of 71.1%. The statistic of the overall accuracy of the combined WBD of the amplitude and the coherence thresholding is similar to them of the amplitude derived water mask.

Concluding, the classification based on the amplitude image represents very well smooth water bodies and is very rich in detail with displaying even small feeder rivers as water bodies. However, some patches detected mainly with the weak threshold are not supposed to be water at all but wet or snow covered fields instead. Consequently, the percentage of misclassifications is higher especially with the weak amplitude threshold. The classification based on the coherence image in comparison is showing water bodies that are very reliable but the result is not that rich in detail as the classification result based on the amplitude image.

C. Global Evaluation of Scene-Based Water Body Detection Mask With SWBD

Besides the evaluation of the two test sides mentioned above, a global evaluation of the WBD is implemented. Totally, 840 scenes randomly distributed all over the world have been assessed. SWBD is used as reference data due to its global availability below 60° latitude. Consequently, statistics above 60° latitude are not available. The resolution of SWBD is 30 m, i.e. 1 arc second. Completeness and correctness were calculated for the amplitude derived WBD, the coherence derived WBD and the combined WBD of the amplitude and coherence thresholding by union. The results are classified in three different physical climate zones. The climate zones base on the Köppen climate classification according to their degree of latitudes. The first classification is the equatorial climate from 0–15° latitudes, the second one comprises the dry climates from 15°–35° latitudes and the last one the temperate and snow climates from 35°–60° latitudes. Table II shows the results of the statistic. It is obvious that the values are mostly minor than the ones of the two test sides near Hamburg and Orlando. Compared to the high resolution of ATKIS and NHD reference layer, SWBD is only available in a coarser resolution. Additionally, the different acquisition time of reference data and the TanDEM-X scenes may not be neglected. The WBD derived separately of amplitude and coherence reaches a completeness of 70.1% up to 80.7% disregarding the result for the coherence derived water mask between 35° and 60° latitudes. The correctness achieves a value of 52.5% up to 71.7%. In the equatorial climates the amplitude and the coherence derived water body detection mask shows the best result. Experiences showed that in this climate zone the coherence derived WBD is very accurate, reliable and robust. Equally the differentiation between dark water areas and bright land areas in the amplitude images leads to reliable results. In the warm temperate and snow climates the statistical values for the amplitude derived water mask are constant. In this climate mountainous and agricultural areas are often misclassified with the weak amplitude threshold. This leads to a minor correctness compared to the one of the coherence derived water mask.

TABLE II
EVALUATION RESULTS FOR THE SCENE-BASED WATER BODY DETECTION DERIVED OF AMPLITUDE, COHERENCE AND THE COMBINED AMPLITUDE AND COHERENCE THRESHOLDING OF 840 GLOBALLY RANDOMLY DISTRIBUTED TEST SITES IN COMPARISON WITH SWBD: EQUATORIAL CLIMATE BETWEEN 0 TO 15° LATITUDES, DRY CLIMATES BETWEEN 15° TO 35° LATITUDES AND WARM TEMPERATE AND SNOW CLIMATES BETWEEN 35° TO 60° LATITUDES

	Latitudes	Number of scenes	Completeness	Correctness
Amplitude	0°-15°	201	75.0	71.3
	15°-35°	218	72.4	52.5
	35°-60°	421	73.0	54.5
Coherence	0°-15°	201	80.7	71.7
	15°-35°	218	70.1	60.6
	35°-60°	421	60.4	66.3
Amplitude + Coherence	0°-15°	201	85.6	67.5
	15°-35°	218	81.4	51.3
	35°-60°	421	76.2	51.8

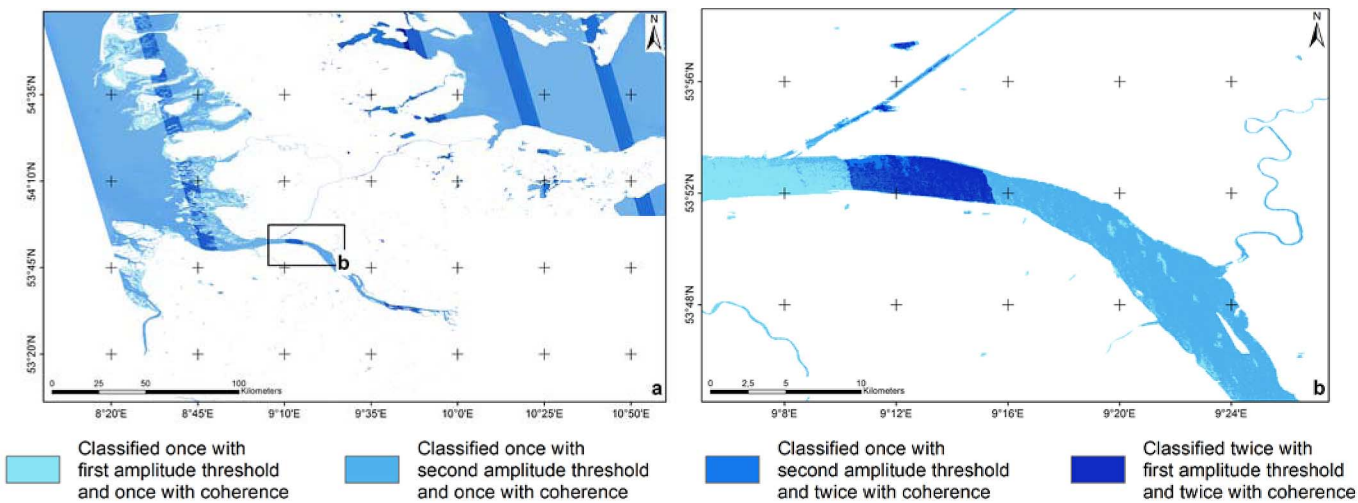

Fig. 5. (a) Water Indication Mask at the German Bight: mosaicked result of 46 input water body detection masks which were acquired between 20th October 2010 and 9th December 2011 covering an area of 2° × 3° containing the result of the amplitude threshold and the coherence threshold. The darker the blue, the oftener the pixel is classified as water. (b) Subset of the Water Indication Mask of the river Elbe (black rectangle in (a)).

Though frozen water areas lead to a high coherence. In this case the coherence thresholding cannot be used for classifying water areas. In contrast to the amplitude, the completeness of the coherence derived water mask decreases to 60.4%, the correctness however increases to 66.3%. The last three rows of Table II show the overall accuracy of the combined WBD. The completeness increases in all three climates to 76.2% and 85.2%. Therefor the correctness decreases to 51.3% and 67.5%. In total, the statistics prove that dependent on climate, land cover or application, the amplitude and/or the coherence derived water body detection mask must be chosen in order to achieve the best classification for accurate water body detection.

D. Evaluation of the Final Water Indication Mask

Fig. 5(a) shows the WAM of North Germany covering an area of 2° × 3°. Totally, 46 WBD have been mosaicked to a single WAM. The data were acquired from 20th October until 9th December 2011. In the figure, all detected water is delineated in blue. The different blue colours originate from the different classification results explained in Section V-B, e.g. the first light blue in the legend stands for classified once with the first, reliable amplitude threshold and once with the coherence threshold etc. The darker the blue, the oftener the pixel is classified as water in different WBD in amplitude and coherence image. The border between ocean and coast line is accurately and continuously illustrated. The water in the North Sea is partially lighter. Due to temporal changes the water is not classified in all information layers. With the frequency of occurrence in the different threshold detections this outlier can be minimized. The stripes which are displayed in a darker blue are the overlapping areas of different acquisitions. A subset of an overlap is shown in Fig. 5(b) using the WAM at the river Elbe. In the dark blue area the pixel is classified twice as water, in the neighbouring data take the pixel is only classified once as water and hence delineated in a lighter blue. The result of the WAM is accurate. Especially for the river Elbe, the WAM of the amplitude image and coherence images are similar. Consequently, both information layers can be used for the subsequent DEM editing. In this purpose, especially the information of the coherence image is valuable as incoherent areas indicate where the DEM is noisy and needs to be filtered or flattened. For other applications, the information of amplitude and coherence image could be used jointly. An evidence of the accuracy would not be very meaningful because it depends on the selection of the required information and hence on the application.

Fig. 6(a) shows the TanDEM-X DEM with unedited water areas. Since the classifications of the amplitude and the coherence analysis of the river Elbe are similar, the combined WAM

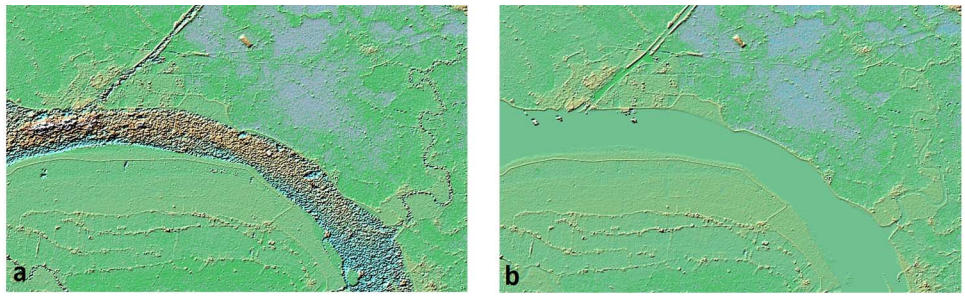

Fig. 6. (a) TanDEM-X DEM with unedited water areas of the first study area around the river Elbe in the west of Hamburg, Germany, (b) TanDEM-X DEM with edited water areas of the first study area around the river Elbe in the west of Hamburg, Germany.

can be used for the DEM editing. Fig. 6(b) presents the result of the DEM after editing. Now, the water areas are flat and on the same levelling. For the direction of flow the terrain is considered. Hence the edited DEM can be used for a lot of applications like ortho-rectification of remote sensing data or any geo-application like hydrological modelling.

VI. Conclusion

The purpose of the Water Indication Mask is to support a TanDEM-X-DEM editing process. It comprises the combination of data sets acquired at different dates with time spans up to a year. In between, the appearance of water bodies can vary due to tides, flooding, seasonally changing water levels, rain fall or aridity, snow and ice coverage and even phenological effects. Therefore, the generation of the Water Indication Mask is split into an analysis of every single interferometric data set and a mosaicking and fusion of the individual results to the final Water Indication Mask.

The extraction of water bodies from a single TanDEM-X scene relies on a threshold method applied on amplitude as well as on coherence images. In particular the information of the coherence image is valuable as incoherent areas indicate where the DEM is noisy and needs to be filtered or flattened. For the amplitude thresholding two different threshold values are selected in order to capture the variations of the appearance of water. The quality of the resulting scene-based product was determined by a comparison with reference data. Water bodies were derived from the amplitude image with correctness up to 92.5%. The correctness of the coherence based analysis was up to 98.7%. It is more reliable but less rich in detail. The comparison of the 840 randomly distributed water bodies showed that the methodology is globally applicable and very accurate. The correctness was up to 71.3% and 71.7%. The results differ depending on land cover and climate. However, with a precise selection of the amplitude or coherence derived water body detection mask the accuracy can be improved.

The mosaicking and fusion of the scene-based products is performed by counting for every pixel of the final Water Indication Mask how often the individual amplitude and coherence thresholds indicate the existence of water at that position. The higher the frequency of classification, the more reliable the pixel represents water. The combination of different information layers helps to compensate missing classification results due to temporal changes, coherent water or missing SAR backscattering. The WAM do not present a complete water mask. But with a precise, sophisticated selection of the classification result it can be used for a helpful indication of water bodies or for the finding of an accurate border between coast line and ocean. With a posting of 12 m and a global coverage, the WAM will be an outstanding information layer.

References

[1] G. Krieger, A. Moreira, H. Fiedler, I. Hajnsek, M. Werner, M. Younis, and M. Zink, "TanDEM-X: A satellite formation for high resolution SAR interferometry," *IEEE Trans. Geosci. Remote Sens.*, vol. 45, no. 11, pp. 3317–3341, Nov. 2007.

[2] R. Richter and D. Schläpfer, "Geo-atmospheric processing of airborne imaging spectrometry data. Part 2: Atmospheric/topographic correction," *Int. J. Remote Sens.*, vol. 23, no. 13, pp. 2631–2649, 2002.

[3] M. Huber, B. Wessel, and A. Roth, "The TerraSAR-X orthorectification service and its benefit for land use applications," in *Proc. IEEE Int. Geoscience and Remote Sensing Symp. (IGARSS'06)*, Jul. 2006, pp. 1922–1925.

[4] S. P. Wechsler, "Uncertainties associated with digital elevation models for hydrologic applications: A review," *Hydrol. Earth Syst. Sci.*, vol. 11, pp. 1481–1500, Aug. 2007.

[5] R. Ludwig and P. Schneider, "Validation of digital elevation models from SRTM X-SAR for applications in hydrologic modelling," *J. Photogramm. Remote Sens.*, vol. 60, pp. 339–358, 2006.

[6] B. Wessel, U. Marschalk, A. Gruber, M. Huber, T. Hahmann, and A. Roth, "Design of the DEM mosaicking and calibration processor for TanDEM-X," in *Proc. European Conf. Synthetic Aperture Radar (EUSAR'08)*, Jul. 2008, vol. 7, pp. 111–114.

[7] H. Breit, T. Fritz, M. Eineder, R. Bamler, M. Lachaise, R. Brcic, N. Adam, and N. Yague-Martinez, "Processing system and algorithm for the TanDEM-X mission," in *Proc. IEEE Int. Geoscience and Remote Sensing Symp. (IGARSS'09)*, Jul. 2009, p. 4.

[8] A. Wendleder, M. Breunig, K. Martin, B. Wessel, and A. Roth, "Water body detection from TanDEM-X data: Concept and first evaluation of an accurate water indication mask," in *Proc. IEEE Int. Geoscience and Remote Sensing Symp. (IGARSS'11)*, Jul. 2011, p. 4.

[9] M. Huber, A. Gruber, B. Wessel, M. Breunig, and A. Wendleder, "Validation of the tie-point concepts by the DEM adjustment approach of TanDEM-X," in *Proc. IEEE Int. Geoscience and Remote Sensing Symp. (IGARSS'10)*, Jul. 2010, pp. 2644–2647.

[10] A. Gruber, B. Wessel, and M. Huber, "TanDEM-X DEM calibration: Correction of systematic DEM errors by block adjustment," in *Proc. IEEE Int. Geoscience and Remote Sensing Symp. (IGARSS'09)*, Jul. 2009, p. 4.

[11] TanDEM-X Ground Segment, TanDEM-X DEM Product Specification, TD-GS-PS-0021, no. 1.8, Apr. 2011.

[12] S. Cloude and K. Papathanassiou, "Polarimetric SAR interferometry," *IEEE Trans. Geosci. Remote Sens.*, vol. 36, no. 5, pp. 1551–156, 1998.

[13] R. Bamler and P. Hartl, "Synthetic aperture radar interferometry," *Inverse Problems*, vol. 14, no. 4, pp. R1–R54, 1998.

[14] T. Hahmann, A. Twele, S. Martinis, and M. Buchroithner, "Strategies for the automatic extraction of water bodies from TerraSAR-X/TanDEM-X Data," *Geographic Information and Cartography for Risk and Crisis Management, Towards Better Solutions*, pp. 129–141, 2010.

[15] T. G. Farr, P. A. Rosen, E. Caro, R. Crippen, R. Duren, S. Hensley, M. Kobrick, and M. Paller *et al.*, "The shuttle radar topography mission," *Rev. Geophys.*, vol. 45, p. RG2004, 10.1029/2005RG000183.

[16] S. Martinis, A. Twele, and S. Voigt, "Towards operational near real-time flood detection using a split-based automatic thresholding procedure on high resolution TerraSAR-X data," *Natural Hazards Earth Syst. Sci.*, vol. 9, pp. 303–314, 2009.
[17] T. Hahmann, A. Roth, S. Martinis, A. Twele, and A. Gruber, "Automatic extraction of water bodies from TerraSAR-X data," in *Proc. IEEE Int. Geoscience and Remote Sensing Symp. (IGARSS'08)*, Jul. 2008, pp. III-103–III-106.
[18] M. S. Horritt, D. C. Mason, and A. J. Luckmann, "Flood boundary delineation from synthetic aperture radar imagery using a statistical active contour model," *Int. J. Remote Sens.*, vol. 22, no. 13, pp. 2489–2507, 2001.
[19] T. Hahmann and B. Wessel, "Surface water body detection in high-resolution TerraSAR-X data using active contour models," in *Proc. European Conf. Synthetic Aperture Radar (EUSAR)*, 2010, vol. 8, p. 4.
[20] M. Silveira and S. Heleno, "Separation between water and land in SAR images using region-based level sets," *IEEE Geosci. Remote Sens. Lett.*, vol. 6, no. 3, pp. 471–475, Jul. 2009.
[21] G. Nico, M. Pappalepore, G. Pasquariello, A. Refice, and S. Samarelli, "Comparison of SAR amplitude vs. coherence flood detection methods—A GIS application," *Int. J. Remote Sens.*, vol. 21, no. 8, pp. 1619–1631, 2000.
[22] C. Hall-Atkinson and L. C. Smith, "Delineation of delta ecozones using interferometric SAR phase coherence Mackenzie River delta, N.W.T., Canada," *Remote Sens. Environ.*, vol. 78, pp. 229–238, 2001.
[23] V.-P. Onana, E. Trouvé, G. Mauris, J.-P. Rudant, and E. Tonyé, "Linear features extraction in rain forest context from interferometric SAR images by fusion of coherence and amplitude information," *IEEE Trans. Geosci. Remote Sens.*, vol. 41, no. 11, pp. 2540–2556, 2003.
[24] R. Romeiser, H. Breit, M. Eineder, and H. Runge, "Demonstration of current measurements from space by along-track SAR interferometry with SRTM data," in *Proc. IEEE Int. Geoscience and Remote Sensing Symp. (IGARSS)*, 2002, pp. 158–160.
[25] J. Kittler and J. Illingworth, "Minimum error thresholding," *Pattern Recogn.*, vol. 19, pp. 41–47, 1986.
[26] TerraSAR-X Ground Segment, Level 1b Product Format Specification, TX-GS-DD-3307, no. 1.3, Dec. 2007.
[27] National Aeronautics and Space Administration (NASA), SRTM Water Body Data Product Guidance, vol. 2, p. 4, 2003.
[28] J. A. Slater, G. Garvey, C. Johnston, J. Haase, B. Heady, G. Kroenung, and J. Little, "The SRTM data "finishing" process and products," *Photogramm. Eng. Remote Sens.*, vol. 72, no. 3, pp. 237–247, 2006.
[29] E. Bribiesca, "A new chain code," *Pattern Recogn.*, vol. 32, pp. 235–251, 1999.
[30] F. Trautwein, J. Fisler, M. Hugentobler, P. Lüscher, R. Weibel, and S. Hägi, "Geländeanalyse," *Geographic Information Technology Training Alliance (GITTA)*, vol. 5, p. 25, 2011.
[31] United States Geological Survey,, The National Hydrography Dataset, 2000.

Anna Wendleder received a diploma degree in geodesy from the Technical University of Munich (TUM), Germany, in 2008.

Since 2008, she has been a research associate at the German Remote Sensing Data Center (DFD), German Aerospace Center (DLR). Her research focuses on SAR remote sensing including image analysis and geocoding.

Birgit Wessel received a diploma degree in geodesy from the University of Hanover, Germany, in 2000 and a Dr.-Ing. degree from the Technical University of Munich (TUM), Germany, in 2006.

From 2000 to 2005, she was a scientific collaborator at the Institute for Photogrammetry and Cartography at the TUM, where she was working on her Ph.D. on "Automatic Extraction of Roads from SAR images". Since 2005 she has been with the German Remote Sensing Data Center, German Aerospace Center (DLR), where she currently is leading the DEM calibration and mosaicking developments for the German interferometric TanDEM-X satellite mission. Her research focuses on SAR remote sensing including image analysis, characterization of objects and geocoding.

Achim Roth received the degree as graduate engineer in geodesy from the University of Karlsruhe, Germany, in 1987.

He joined the German Aerospace Centre in 1987 for the development and implementation of an operational SAR geocoding system for the ERS- and X-SAR-missions. Since 1991 he is leading the team "SAR Topography" at DLR's German Remote Sensing Data Center (DFD). From 2000 until 2004 he was the SRTM/X-SAR Ground Segment Manager. Since 2002 he is the TerraSAR-X Science Coordinator. The team's research focuses on the development of geo-information products, the corresponding retrieval techniques and their implementation as operational processors. It contributed to the Shuttle Radar Topography Mission (SRTM) and is currently involved in the TerraSAR-X and TanDEM-X missions.

Markus Breunig received a diploma degree in geography from the University of Würzburg, Germany, in 2008.

Since 2009, he has been a research associate at the German Remote Sensing Data Center (DFD), German Aerospace Center (DLR). His work focuses on the operation, system monitoring and quality control within the DEM preparation, calibration and mosaicking processors for the TanDEM-X mission.

Klaus Martin received a Ph.D. from the Technical University Munich (TUM), Munich, Germany, in 1994.

Since 1980 he has been head of the Company for Remote Sensing and Environmental Research (SLU) in Munich. His fields of experience include remote sensing and GIS for mapping and monitoring land cover and use.

Susanne Wagenbrenner received a diploma degree in geography from the University of Würzburg, Germany, in 2008.

Since 2011, she has been a research associate at the Company for Remote Sensing and Environmental Research (SLU). Her work focuses on the operation, system monitoring and quality control within the DEM preparation, calibration and mosaicking processors for the TanDEM-X mission.